measured data (*11*). Finally, a possible complication of the results derived in this work may be that the cross section possesses a pronounced dependence on rotation of the molecule. However, Amano (*14*) has investigated the dependence of the reaction rate on rotation between 110 and 273 K and concluded that the rotational dependence is very small or negligible. This does not, of course, exclude a speculative possibility of a stronger rotational dependence for rate coefficients at very low temperatures.

REFERENCES AND NOTES

1. T. Oka and M.-F. Jagod, *J. Chem. Soc. Faraday Trans.* **89**, 2147 (1993).
2. D. Smith, *Philos. Trans. R. Soc. London Ser. A* **324**, 257 (1988).
3. P. Drossart *et al.*, *Nature* **340**, 539 (1989).
4. S. J. Kim *et al.*, *ibid.* **353**, 536 (1991).
5. R. Baron *et al.*, *ibid.*, p. 539.
6. L. M. Trafton *et al.*, *Astrophys. J.*, in press.
7. S. Miller, J. Tennyson, S. Lepp, A. Dalgarno, *Nature* **355**, 420 (1992).
8. If the rate for dissociative recombination is high, then it is the main destruction mechanism of H_3^+. For a general reference, see, for instance, A. Dalgarno and J. H. Black, *Rep. Prog. Phys.* **39**, 573 (1976).
9. A. Dalgarno, in preparation.
10. E. F. van Dishoeck, in *Molecular Astrophysics*, T. W. Hartquist, Ed. (Cambridge Univ. Press, Cambridge, 1990), pp. 55–83.
11. M. Larsson *et al.*, *Phys. Rev. Lett.* **70**, 430 (1993).
12. M. T. Leu, M. A. Biondi, R. Johnsen, *Phys. Rev. A* **8**, 413 (1973).
13. N. G. Adams, D. Smith, E. Alge, *J. Chem. Phys.* **81**, 1778 (1984).
14. T. Amano, *ibid.* **92**, 6492 (1990).
15. A. Canosa, B. R. Rowe, J. B. A. Mitchell, J. C. Gomet, C. Rebrion, *Astron. Astrophys.* **248**, L19 (1991).
16. A. Canosa *et al.*, *J. Chem. Phys.* **97**, 1028 (1992).
17. N. G. Adams and D. Smith, in *Astrochemistry*, M. S. Vardya and S. P. Tarufdar, Eds. (Reidel, Dordrecht, Netherlands, 1987), pp. 1–18. The very low rate of $\sim 10^{-11}$ cm^3 s^{-1} claimed in this report has recently been revised to 10^{-8} to 2×10^{-8} cm^3 s^{-1} at 300 K [D. Smith and P. Spanel, *Chem. Phys. Lett.* **211**, 454 (1993)].
18. J. A. Macdonald, M. A. Biondi, R. Johnsen, *Planet. Space Sci.* **32**, 651 (1984).
19. D. Auerbach *et al.*, *J. Phys. B* **10**, 3797 (1977).
20. D. Mathur, S. U. Khan, J. B. Hasted, *ibid.* **11**, 3615 (1978).
21. B. Peart and T. Dolder, *ibid.* **7**, 1948 (1974).
22. H. Hus, F. B. Youssif, A. Sen, J. B. A. Mitchell, *Phys. Rev. A* **38**, 658 (1988).
23. K. C. Kulander and M. F. Guest, *J. Phys. B* **12**, L501 (1979); H. H. Michels and R. H. Hobbs, *Astrophys. J.* **286**, L27 (1984); J. N. Bardsley, *J. Phys. B* **1**, 365 (1968).
24. D. R. Bates, M. F. Guest, R. A. Kendall, *Planet. Space Sci.* **41**, 9 (1993); D. R. Bates, *Comments At. Mol. Phys.* **29**, 53 (1993).
25. S. Datz and M. Larsson, *Phys. Scr.* **46**, 343 (1992).
26. D. R. DeWitt *et al.*, in preparation.
27. H. Danared, *Phys. Scr.* **48**, 405 (1993).
28. L. Andersen and J. Bolko, *Phys. Rev. A* **42**, 1184 (1990).
29. For the detailed analysis, see a forthcoming publication by J. R. Mowat (in preparation).
30. This result corresponds to $kT_\perp = 0.125$ eV. When we take into account the uncertainty in electron temperature, we find $\sigma = (1.43 \pm 0.02) \times 10^{-16}/E^{(1.15 \pm 0.02)}$ cm^2, where the minus sign refers to $kT_\perp = 0.1$ eV and the plus sign to $kT_\perp = 0.15$ eV. In a previous paper (*11*), we represented the cross section at a higher energy range ($E > 0.0025$ eV) by a curve with an energy dependence according to $1/E^{1.44}$. However, the $1/E^{1.44}$ curve should merely be regarded as an attempt to describe the cross section up to 1 eV of collision energy and should not be used to deduce a reaction rate. To avoid confusion, we emphasize that figure 4 in (*11*) represents average cross section, $\langle v\sigma \rangle / v$, which practically equals the cross section σ for $E > 0.1$ eV.
31. E. P. Wigner, *Phys. Rev.* **73**, 1002 (1948).
32. J. Wm. McGowan *et al.*, *Phys. Rev. Lett.* **42**, 373 (1979).
33. A. E. Orel and K. C. Kulander, private communication.

34. The authors thank A. E. Orel and K. C. Kulander for communicating results from calculations of the cross section before publication and D. Belkic for valuable discussions regarding the energy dependence of cross sections, in particular concerning the paper by Wigner (*31*). This work was supported by the Göran Gustafsson Foundation and the Swedish Natural Science Research Council. J.R.M. was supported by NSF, and S.D. was sponsored by the U.S. Department of Energy, Office of Basic Energy Sciences, Division of Chemical Sciences, under contract DE-AC05-84OR21400 with Martin Marietta Energy Systems, Inc.

7 September 1993; accepted 23 November 1993

Hubble Space Telescope Observations of Comet P/Shoemaker-Levy 9 (1993e)

H. A. Weaver,* P. D. Feldman, M. F. A'Hearn, C. Arpigny, R. A. Brown, E. F. Helin, D. H. Levy, B. G. Marsden, K. J. Meech, S. M. Larson, K. S. Noll, J. V. Scotti, Z. Sekanina, C. S. Shoemaker, E. M. Shoemaker, T. E. Smith, A. D. Storrs, D. K. Yeomans, B. Zellner

The Hubble Space Telescope observed the fragmented comet P/Shoemaker-Levy 9 (1993e) (P indicates that it is a periodic comet) on 1 July 1993. Approximately 20 individual nuclei and their comae were observed in images taken with the Planetary Camera. After subtraction of the comae light, the 11 brightest nuclei have magnitudes between ~23.7 and 24.8. Assuming that the geometric albedo is 0.04, these magnitudes imply that the nuclear diameters are in the range ~2.5 to 4.3 kilometers. If the density of each nucleus is 1 gram per cubic centimeter, the total energy deposited by the impact of these 11 nuclei into Jupiter's atmosphere next July will be ~4 × 10^{30} ergs (~10^8 megatons of TNT). This latter number should be regarded as an upper limit because the nuclear magnitudes probably contain a small residual coma contribution. The Faint Object Spectrograph was used to search for fluorescence from OH, which is usually an excellent indicator of cometary activity. No OH emission was detected, and this can be translated into an upper limit on the water production rate of ~2 × 10^{27} molecules per second.

In late March of 1993, a string of comet-like bodies was discovered near Jupiter (*1*). Subsequent observations showed convincingly that this object, comet P/Shoemaker-Levy 9 (1993e), made a close approach (~1.4 R_J; R_J is Jupiter's radius) to Jupiter in July 1992, at which time tidal forces broke the parent body into numerous fragments, which now follow slightly different orbits (*2*). Integration of these orbits forward in time shows that all of the major fragments in the comet will almost certainly impact Jupiter's atmosphere over an approximately 6-day period centered on 20 July 1994. Because the fragments will be traveling rapidly (~60 km s^{-1}) as they enter Jupiter's atmosphere, the impact could be spectacular. Although the impacts are predicted to occur on the hemisphere that is unobservable from Earth, the effects on the atmosphere will probably still be visible as the impact zone rotates into Earth's view (Jupiter's rotation period is 9.84 hours).

The energy deposited into Jupiter's atmosphere by each impacting body is proportional to the cube of its size, so it is important to obtain the best possible size estimates. The Hubble Space Telescope (HST) has the highest spatial resolution of

H. A. Weaver, R. A. Brown, K. S. Noll, T. E. Smith, A. D. Storrs, Space Telescope Science Institute, 3700 San Martin Drive, Baltimore, MD 21218, USA.
P. D. Feldman, Department of Physics and Astronomy, The Johns Hopkins University, Baltimore, MD 21218, USA.
M. F. A'Hearn, University of Maryland, Department of Astronomy, College Park, MD 20742, USA.
C. Arpigny, Université de Liège, Institut d'Astrophysique, B-4000 Liège, Belgium.
E. F. Helin, Z. Sekanina, D. K. Yeomans, Jet Propulsion Laboratory, Pasadena, CA 91109, USA.
D. H. Levy, S. M. Larson, J. V. Scotti, University of Arizona, Lunar and Planetary Laboratory, Tucson, AZ 85721, USA.
B. G. Marsden, Harvard-Smithsonian Center for Astrophysics, Cambridge, MA 02138, USA.
K. J. Meech, University of Hawaii, Institute for Astronomy, Honolulu, HI 96822, USA.
C. S. Shoemaker, Northern Arizona University, Department of Physics and Astronomy, Flagstaff, AZ 86011, USA.
E. M. Shoemaker, U.S. Geological Survey, Flagstaff, AZ 86001, USA.
B. Zellner, Astronomy Programs, Computer Sciences Corporation, c/o Space Telescope Science Institute, Baltimore, MD 21218, USA.

*To whom correspondence should be addressed.

any currently available optical telescope, and we report here on HST images of 1993e taken with the Planetary Camera (PC).

That 1993e is a fragmented comet, as opposed to a fragmented asteroid, is suggested by the probable low tensile strength of the parent body [~200 to 1500 dyne cm^{-2} (3)] and the appearance of a dust tail. The presence of a nearly circular coma around each nucleus also suggests a cometary origin, because outgassing from the nucleus could easily produce such a morphology, and tidal splitting seems to place fragments primarily along a line (as projected on the sky). Probably the most convincing demonstration that 1993e is a comet would come from the detection of volatiles, because asteroids are generally expected to be less icy than comets. Thus, in addition to our imaging program with the PC, we have used the Faint Object Spectrograph (FOS) on HST to search for ultraviolet (UV) fluorescence from OH, which is usually the strongest emission feature in the UV-optical spectra of comets.

In the HST images, at least 11 nuclei are clearly detected (Fig. 1A). Eight others are presumed real because they appear in two or more independent images. There are several other marginal candidate nuclei, but more HST observations are needed to verify their existence.

Jewitt, Luu, and Chen (4) detected 21 nuclei in their ground-based images of 1993e using the University of Hawaii 2.2-m telescope (the HST is a 2.4-m telescope). Although HST's spherical aberration degrades our ability to detect faint nuclei, there appears to be no significant difference between the number of nuclei detected in the two observations. The correspondence between the two sets of identified nuclei is excellent.

Scattered sunlight from the dust coma is responsible for most of the signal observed in both the ground-based and HST images. The higher resolution of HST gives increased contrast between the nucleus and the coma, making it easier to extract the true nuclear magnitudes, which can then provide better estimates for the nuclear sizes. High spatial resolution is also clearly an advantage in separating closely spaced nuclei. The region near the center of Fig. 1B contains at least four nuclei, which merge into a single elongated feature at lower spatial resolution.

To investigate the coma morphology in detail, we extracted radial brightness profiles for the brightest nuclei and calculated spatial profiles for a model point spread function (PSF) and a ρ^{-1} brightness distribution convolved with the PSF (where ρ is the projected distance to the nucleus) (Fig. 2). The latter is the profile expected for steady-state production of dust flowing outward from a nucleus with constant velocity (5). Examination of Fig. 2 demonstrates clearly that the "fuzz" around each nucleus is true coma and not an artifact produced by HST's spherical aberration. Even if the PSF (that is, the nucleus) is responsible for all of the flux measured in the peak pixel, it makes only a small contribution to the flux observed in neighboring pixels.

Typical cometary dust comae have spatial brightness distributions that follow approximately a ρ^{-1} profile, or are slightly steeper (6), but the comae surrounding the individual nuclei in 1993e are flatter. The dust surrounding the nuclei is apparently not from steady-state production at the nucleus followed by constant velocity outflow and may instead be a population of relatively large grains that are essentially

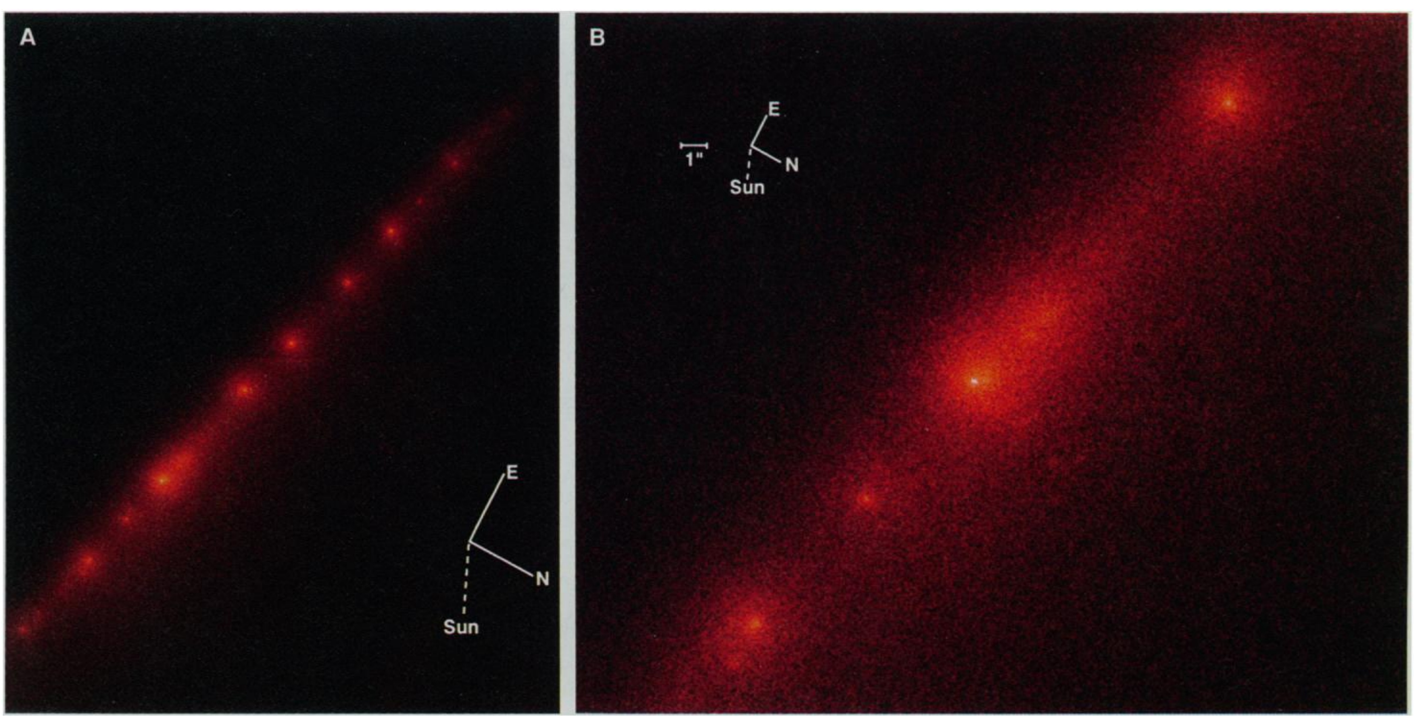

Fig. 1. An image of comet P/Shoemaker-Levy 9 taken with the HST PC between 0700 and 1200 UTC on 1 July 1993 with the F555W filter (similar to *V* band). The comet's heliocentric distance was 5.45 astronomical units (AU), the geocentric distance was 5.46 AU, the heliocentric radial velocity was -0.45 km s^{-1}, and the phase angle was 10.7°. Three separate images, with exposure times of 400, 700, and 700 s, were calibrated separately [by the procedures described by Lauer (*17*)] and then co-aligned and averaged to produce the image shown here. Pixel intensities that were significantly different ($\geq 3\sigma$, where σ is derived from an accurate noise model of the PC) from the median value for the three images were not used in the average to eliminate cosmic-ray contamination. (**A**) A 1450 × 1450 pixel image showing the entire train. (**B**) A 565 × 565 pixel region in the vicinity of the brightest nucleus. The pixels are square, 0.0439 arc sec on a side, which projects to an area 174 km wide at the distance of 1993e. At low spatial resolution, the area near the center of (B) appears as a single elongated feature but is seen in the HST data to be at least four individual nuclei. These nuclei do not fall along the line that almost connects most of the other nuclei. The projected separation of the brightest nucleus and its apparent companion is ~1100 km. The compass gives the directions of celestial north (N), celestial east (E), and the projected vector to the sun (Sun).

unaffected by solar radiation pressure and, thus, have orbits quite similar to those of their parent nuclei. If so, this dust debris should still be visible during future observations.

To extract magnitudes for the individual nuclei, one must first subtract the flux from the coma. We used a simple iterative procedure to accomplish this. First, a model PSF was formed whose peak pixel intensity equaled the observed peak pixel intensity. Integration of the signal from this PSF clearly overestimated the true nuclear flux because some fraction of the peak pixel intensity must be nonnuclear. Second, the background was estimated by subtracting the total flux in a 3 by 3 pixel box centered on the brightest pixel of the initial PSF from the total flux in the same part of the observed image and then averaging per pixel. This gave the background contribution (coma and any residual sky) to the observed peak pixel intensity, assuming it to be constant over the 3 × 3 box. Third, the background was subtracted from the observed peak pixel intensity to give a new estimate for the point source contribution to the peak pixel. The PSF was renormalized to this new peak pixel value, and steps 2 and 3 were repeated. The process converged after ~15 iterations. Applying this method to two of the brighter nuclei (11 and 15 in Table 1), we found that the nucleus contributed ~30% of the peak pixel intensity and only ~15% of the total flux observed in the 3 × 3 box. We take these percentages to be valid for all the nuclei because the spatial brightness profiles and visual appearances of the bright nuclei are similar. Because the peak pixel intensity can vary by about ±10%, depending on the source's position on the chip and its position relative to the center of a pixel, these effects alone produce an error of at least this amount in the derived nuclear magnitudes.

For each bright nucleus, the signal contained in a 3 × 3 box was multiplied by 0.15 to get the nuclear contribution; this was then divided by 0.089 to get the total nuclear flux, because our analysis of many HST model PSFs shows that 8.9 ± 0.2% of the total flux from a point source is contained in a 3 × 3 box centered on the brightest pixel. The total nuclear flux was converted to V magnitude [or V, the apparent magnitude measured in the V band (visual, or yellow, light)] with standard formulas (7, 8). Starting from the southwest end of the image and moving northeast, the V magnitudes of the 11 brightest nuclei are listed in Table 1, with an estimated relative error of ~0.1 mags.

The absolute accuracy of these magnitudes depends on the accuracy of the coma subtraction. We performed numerical experiments to test our iterative procedure. For a point source placed on a flat background, the procedure gives the correct result, even when the point source contributes only a small fraction of the peak pixel intensity. When the background has a peak near the nucleus, however, the procedure underestimates the coma brightness at the nucleus and overestimates the contribution from the point source. For a ρ^{-1} brightness profile, our procedure overestimates the nuclear brightness by about a factor of 2. Because the observed surface brightness profiles are flatter than ρ^{-1}, we conclude that our iterative procedure probably overestimates the nuclear brightness by less than a factor of 2. Thus, the nuclear magnitudes in Table 1 are lower limits, but the true values are unlikely to be larger by more than ~0.75 mag.

The nuclear magnitudes can be used to calculate the effective diameter of the nuclei by (9)

$$\left(\frac{d}{2}\right)^2 = \frac{10^{0.4(V_\odot - V + 5\log R\Delta + \beta\alpha)}}{A_p} \quad (1)$$

where d is the nuclear diameter in astronomical units (AU), $V_\odot$ is the solar visual magnitude at 1 AU [−26.77 (9)], R is the distance to the nucleus from the sun, Δ is the distance to the nucleus from the Earth, β is the phase law coefficient (in mags per degree; this describes the decrease in brightness as the Earth-object-sun angle changes from 0° to the observed value), α is the solar phase angle (in degrees), and A_p is the visual geometric albedo.

Neither A_p nor β are known for these nuclei. For several cometary nuclei, estimates for A_p lie in the range 0.02 to 0.13 (10); the value usually quoted for comet P/Halley is 0.04. Essentially nothing is known observationally regarding β; for dark asteroids observed at small phase angles, β generally falls between 0.03 and 0.04 mags deg^{-1}.

Diameters for the 11 brightest nuclei were estimated with A_p = 0.04 and β = 0.035 mag deg^{-1} (Table 1). Because the nuclear magnitudes used to calculate the diameters are probably lower limits (see earlier discussion), the listed nuclear diameters are probably upper limits for the adopted albedo and phase law.

If the nuclei have albedos of 0.9, which is the largest A_p for any known planet or

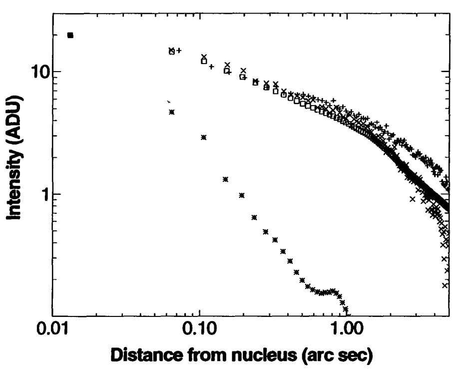

Fig. 2. Azimuthally averaged spatial brightness profiles for one of the well-isolated nuclei (15 in Table 1). The data in two 90° quadrants, whose central axes are approximately perpendicular to the line connecting the nuclei, were used to construct the profiles. For one of the profiles (+), the points are on the sunward side of the line connecting the nuclei, and for the other profile (×), the points are on the opposite side. A constant background level, the estimated residual sky signal, was subtracted from all pixel intensities. The error bars (not shown) on the observed profiles are about the same size as the plotting symbols for points within ~2 arc sec of the nucleus and become slightly larger with increasing distance. Also plotted are radial surface brightness profiles for a model PSF computed for the position of the nucleus (*) and a model ρ^{-1} profile convolved with the PSF (□). ADU, analog-to-digital unit for the charge-coupled device (CCD).

Table 1. Positions, V magnitudes, and diameters of the bright nuclei.

ID*	Position† (arc sec) East	Position† (arc sec) North	V‡	Diameter§ (km)
1	−17.53	−4.68	24.4	3.1
5	−9.27	−2.30	24.2	3.4
6	−4.55	−1.14	24.2	3.4
7	0.00	0.00	23.7	4.3
11	10.71	2.79	23.9	3.9
12	16.43	4.46	23.9	3.9
14	23.75	6.44	24.4	3.1
15	29.58	7.56	23.9	3.8
16	33.15	8.62	24.6	2.9
17	37.71	9.78	24.4	3.0
19	41.53	10.83	24.8	2.5

*Identification numbers were chosen to be compatible with the numbering scheme proposed by Jewitt *et al.* (4). For the nuclei listed above, there is a clear correspondence with those identified in (4). †Relative to the brightest nucleus (#7) in the J2000 system. Because of the roll angle uncertainty of the HST, the errors grow with increasing distance from the reference position at the rate of ~0.010 arc sec per arc min of displacement. The total displacement from the reference nucleus is unaffected by the roll error. The most important sources of error in the measured total displacements are uncompensated field distortion (~0.005 arc sec), chip-to-chip registration errors (~0.04 arc sec when comparing positions on one chip to positions on another), and uncertainty in our ability to define the true nucleus position (the peak pixel intensity or centroid positions may not define accurately the true nuclear positions; this error is probably of order 1 pixel = 0.0439 arc sec). ‡Estimated nuclear V magnitude after coma subtraction. The relative errors are ~0.1 mag. Magnitudes for some of the nuclei might be contaminated by nearby neighbors, but no correction has been attempted because the effect is thought to be small. §Calculated from nuclear V magnitudes with Eq. 1. These diameters are thought to be conservative upper limits to the true values.

satellite (*11*), their diameters would be smaller by a factor of 4.7; therefore, all nuclei would have diameters ≤1 km. The nuclei are unlikely to be more than ~40% larger than the values in Table 1 because the albedos would have to be ≤0.02, currently the lowest value measured for asteroids and cometary nuclei.

With the diameters from Table 1 and a density of 1 g cm^{-3}, the total energy delivered during the impact on Jupiter next July by these 11 nuclei will be $\sim 4 \times 10^{30}$ ergs (= 10^8 megatons of TNT). The largest nucleus alone will deliver $\sim 8 \times 10^{29}$ ergs (= 2×10^7 megatons of TNT). These numbers should be taken as upper limits.

A single parent body 7.7 km in diameter would have the same total volume as these 11 fragments if they are spherical. This parent body, with a geometric albedo of 0.04 and observed near Jupiter at opposition, would have had $V \approx 21.4$, which is ~1 mag fainter than the sensitivity limit reached by a recent observational program designed to search for comets captured by Jupiter (*12*). Apparently, this ground-based search just missed catching 1993e before its breakup.

All the nuclei have comparable sizes, perhaps indicating that the primordial building blocks for the parent body (that is, the planetesimals) were also a few kilometers in diameter (*13*) and that tidal forces from Jupiter simply disassembled the parent body. The HST observations alone, however, do not fully support this conclusion because they are not sensitive to objects smaller than ~2 km, and observations sensitive to diameters well below the HST limit are needed to draw any secure conclusions about the size distribution of nuclear fragments, let alone the planetesimal size distribution. The improved sensitivity expected from the repaired HST will improve the situation, but there will probably still not be enough dynamic range to settle the question.

The spectrum of 1993e shows no evidence for molecular emission. A continuum produced by dust-scattered sunlight was detected and is reddened relative to solar colors by an amount typical of other comets observed in the UV (Fig. 3A). An "emission" spectrum was created by subtracting this continuum (Fig. 3B). If present, the strongest OH band (the [0,0] band of the $A^2\Sigma - X^2\Pi$ system) would appear centered near 3090 Å. The formal limit we derive for the OH brightness is 1.1 ± 0.8 rayleighs (the error is 1σ). Any OH near 1993e presumably arose from the photodissociation of H_2O sublimed from ice in the nuclei or from icy coatings on the dust (or from both).

We used the upper limit on OH emission to estimate how much H_2O is emitted by the comet. We assumed that the H_2O flows radially outward from a point source with a velocity of 0.4 km s^{-1}. The total H_2O lifetime is 2.0×10^6 s (23 days), the H_2O lifetime for dissociation into OH is 2.3×10^6 s, and the lifetime of OH is 4.0×10^6 s (all values were calculated for a heliocentric distance of 5.45 AU). The OH density was calculated by vectorially adding a velocity of 1.05 km s^{-1} (the average OH velocity during the dissociation of H_2O) to the H_2O velocity (*14*). Although 1993e is a spatially extended object with multiple possible source regions of subliming ice, the volatile lifetimes are extremely long, so the spatial brightness distribution of OH should be essentially independent of the exact spatial locations of the sources for H_2O. We derived an upper limit to the H_2O production rate of $\sim 2 \times 10^{27}$ molecules per second (3σ).

This production rate is identical to that estimated for P/Halley at 4.7 AU from the sun preperihelion (*15*), a comet with an effective spherical diameter of ~10 km (*16*). Because only ~10% of Halley's surface area was active [at least near perihelion (*16*)], this comparison indicates that even our short spectroscopic exposure was a fairly sensitive measure of the total amount of icy material in 1993e. However, P/Halley was an unusually bright comet, and most others have significantly smaller H_2O production rates.

We performed a sublimation calculation on a slowly rotating, single nucleus covered with water ice to estimate how large it would have to be to produce the upper limit on the H_2O production rate calculated above. We assumed an infrared emissivity of 0.95 and a visual Bond albedo of 0.04. For such a case, the subsolar surface temperature reaches 170 K and the sublimation rate averaged over the entire surface is $\sim 10^{15}$ molecules per second. The 3σ upper limit of 2×10^{27} molecules per square centimeter per second translates into a nuclear diameter of ~8 km, consistent with the parent body size estimated from the image photometry.

Our basic conclusion is that the largest nuclei in 1993e have diameters of ~2 to 4 km, which is significantly smaller than some earlier estimates. Nevertheless, each of the larger nuclei will deposit 10^{29} to 10^{30} ergs (3×10^6 to 3×10^7 megatons of TNT) into Jupiter's atmosphere next summer. On the basis of our analysis of the spatial brightness profiles and the lack of any molecular emission, we find no evidence for strong cometary activity during the time of the HST observations. Observations early next spring with the refurbished HST should provide a better measurement of the nuclear diameters and a deeper search for cometary activity.

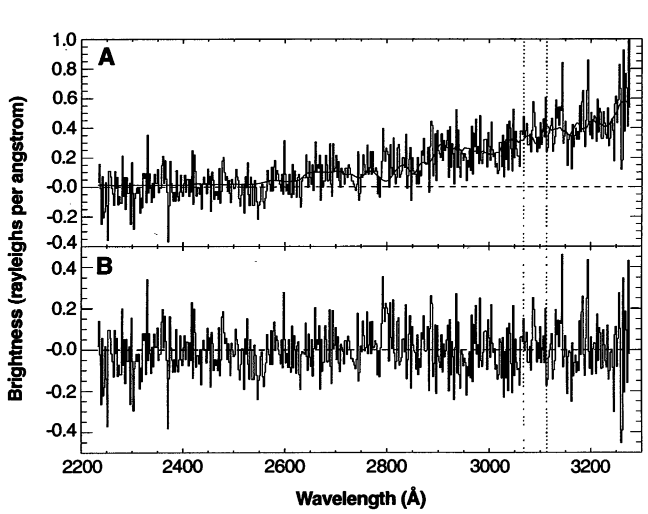

Fig. 3. (**A**) Average 16-min FOS spectrum of the region near the brightest nucleus after subtraction of a flat background (attributable to instrumental dark current). Overplotted is a reddened solar spectrum (*18*) (smooth curve) convolved to the same spectral resolution as the cometary spectrum. (**B**) Difference between the cometary spectrum and the reddened solar spectrum (an "emission" spectrum). Any emission from OH would appear between the dashed lines. An upper limit on the OH brightness is ~2.4 rayleighs (3σ) averaged over the 1.43 by 4.3 arc sec aperture, which can be translated into an upper limit on the water production rate of $\sim 2 \times 10^{27}$ molecules per second.

REFERENCES AND NOTES

1. C. S. Shoemaker, E. M. Shoemaker, D. H. Levy, P. Bendjoya, J. V. Scotti, *Int. Astron. Union Circ. 5725* (1993). Also see J. Luu and D. Jewitt, *Int. Astron. Union Circ. 5730* (1993).
2. J. V. Scotti and H. J. Melosh, *Nature* **365**, 733 (1993); Z. Sekanina, P. Chodas, D. K. Yeomans, in preparation; A. Carusi, B. G. Marsden, G. B. Valsecchi, poster paper presented at *Asteroids, Comets, Meteors 1993*, Belgirate, Italy, 14 to 18 June 1993 (International Astronomical Union Symposium 160). Other orbit information, including early discussions of a possible comet-Jupiter impact, is given in B. G. Marsden, *Int. Astron. Union Circ. 5726* (1993); *Int. Astron. Union Circ. 5744* (1993); and S. Nakano, B. G. Marsden, A. Carusi, *Int. Astron. Union Circ. 5800* (1993).
3. Z. Sekanina, *Science* **262**, 382 (1993).
4. D. Jewitt, J. Luu, J. Chen, *Bull. Am. Astron. Soc.* **25**, 1042 (1993).
5. L. V. Wallace and F. D. Miller, *Astron. J.* **63**, 213 (1958).
6. D. C. Jewitt and K. J. Meech, *Astrophys. J.* **317**, 992 (1987); W. A. Baum, T. J. Kreidl, D. G. Schleicher, *Astron. J.* **104**, 1216 (1992).
7. W. B. Sparks, C. Ritchie, J. Mackenty, *WF/PC Instrument Science Report 92-09*, (Space Telescope Science Institute, Baltimore, MD, 1992).
8. H. C. Harris, W. A. Baum, D. A. Hunter, T. J. Kreidl, *Astron. J.* **101**, 677 (1991).

9. This is a slight modification of the formula appearing in B. Zellner, T. Gehrels, J. Gradie, *ibid.* **79**, 1100 (1974).
10. P. R. Weissman, M. F. A'Hearn, L. A. McFadden, H. Rickman, in *Asteroids II*, R. Binzel, T. Gehrels, M. S. Matthews, Eds. (Univ. of Arizona Press, Tucson, AZ, 1989), pp. 880–920.
11. C. W. Allen, *Astrophysical Quantities* (Athlone, London, ed. 3, 1976), p. 162.
12. G. Tancredi, M. Lindgren, C.-I. Lagerkvist, *Int. Astron. Union Circ. 5892* (1993).
13. V. S. Safronov, "Evolution of the Protoplanetary Cloud and Formation of the Earth and Planets," *NASA TT F-677* (1972) (the original Russian article was published in 1969); P. Goldreich and W. R. Ward, *Astrophys. J.* **183**, 1051 (1973).
14. M. C. Festou, *Astron. Astrophys.* **95**, 69 (1980); J. Crovisier, *ibid.* **213**, 459 (1989).
15. S. Wyckoff, R. M. Wagner, P. A. Wehinger, D. G. Schleicher, M. C. Festou, *Nature* **316**, 241 (1985).
16. H. U. Keller *et al.*, *Astron. Astrophys.* **187**, 807 (1987).
17. T. R. Lauer, *Publ. Astron. Soc. Pac.* **101**, 445 (1989).
18. M. E. Vanhoosier, J.-D. F. Bartoe, G. E. Brueckner, D. K. Prinz, *Astrophys. Lett. Commun.* **27**, 163 (1988).

19. This work is based on observations with the National Aeronautics and Space Administration (NASA)–European Space Agency HST obtained at the Space Telescope Science Institute (STScI), which is operated by the Association of Universities for Research in Astronomy, Inc., under NASA contract NAS5-26555. We thank the acting STScI director at the time of our observations, P. Stockman, for approving our observing time as a Director's Discretionary time program. We also thank the many people at the STScI who were responsible for implementing the program. H.A.W. thanks the Center for Astrophysical Studies at the Johns Hopkins University for its hospitality during his sabbatical visit, during which time the observations were conducted.

19 October 1993; accepted 20 December 1993

Theoretical Evidence for a C_{60} "Window" Mechanism

Robert L. Murry and Gustavo E. Scuseria*

On the basis of semiempirical and high-level ab initio calculations, theoretical evidence is presented of a "window" mechanism operable on the surface of C_{60} and other fullerenes. Through this mechanism, large holes may be formed in fullerenes excited to their triplet state, openings through which atoms and small molecules can pass. This work provides a theoretical foundation for experiments that have prepared endohedral noble gas compounds of C_{60} under thermal excitation. A method is proposed that could increase the efficiency of the process of noble gas insertion into C_{60} and provide a more general means to create endohedral fullerene compounds.

Nature may abhor a vacuum, but fullerene (*1, 2*) researchers find the vacancies inside these hollow carbon cages one of the molecules' most attractive features. The discovery of the metallofullerenes (*3, 4*), fullerenes with metal atoms trapped inside them, was nearly concurrent with that of C_{60} and equally exciting. Numerous metallofullerenes (*5, 6*) have been synthesized by the inclusion of metal sources in the graphite used for fullerene generation, and several noble gases (*7–10*) and small metal atoms (*11*) have also been implanted with ion beam collision experiments. Nevertheless, it seems that only elements with Pauling electronegativities of less than ~1.5 (that is, in general, elements on the left side of the periodic table) are spontaneously trapped inside fullerenes by resistive heating or in arc experiments (*12*), and ion implantation has been limited to He, Ne, Li, Na, and K insertion (*13*). Research into alternative routes to custom-fill the fullerenes' void with a variety of atoms and molecules continues at a rapid rate, for such endohedral species could tailor the physical and chemical properties of fullerenes to specific applications. The filled fullerene cages could have applications as superconductors, drug-delivery agents, medical imaging compounds, or molecular containers. But as of now, no general experimental means for making any X@C_{60} compound exists, and synthesizing endohedral fullerene compounds in macroscopic quantities is difficult at best.

A series of experiments by Saunders *et al.* (*14*) has revealed a method of creating endohedral fullerene compounds. By heating C_{60} soot under atmospheres of He, Ne, Ar, Kr, or Xe to ~600°C for a few hours, significant quantities of He@C_{60} or other noble gas endohedral fullerenes are formed (*14, 15*). Further heating of these endohedral compounds can cause the molecules to release the noble gases, and Saunders *et al.* calculated the Arrhenius activation barrier of helium release to be ~3.5 eV (*14*). Thus, under those relatively mild conditions, a "window" of sorts is formed on the fullerene surface through which the atoms may pass in and out. Because the barrier for direct helium insertion through a six-membered carbon ring is very high (~8.7 eV) (*16, 17*), and barriers for insertion of the other noble gases must be even higher, such a brute force mechanism does not seem to be a satisfying explanation of these experiments.

In this report, on the basis of theoretical calculations, we present evidence for a window mechanism that may occur on the surface of fullerenes. Specifically, we have found that opening the C–C bonds in the fullerene cage to create 9- and 10-membered rings is a relatively low energy process in the triplet state potential energy surface. We have confirmed this theoretical finding both in model fullerene systems and in C_{60}. Furthermore, a minimum exists in the triplet C_{60} potential energy surface with the single C–C bond open to 2.48 Å. We propose that the holes in such metastable species may allow the insertion of atoms and small molecules into the fullerene cage more easily than through direct penetration at the center of a pentagon or hexagon.

The theoretical tools used in this work include the semiempirical MNDO procedure (*18, 19*), the ab initio direct self-consistent field (SCF) Hartree Fock method (*20, 21*), and the local density approximation (LDA) (*22*) and nonlocal Becke-Lee-Yang-Parr (BLYP) (*23, 24*) density functional theory. The SCF method has proven reliable for predicting fullerene structures (*25, 26*), and the BLYP method has been shown to reproduce the experimental thermochemistry of chemical reactions to within a few kilocalories per mole (*23*).

To investigate the energetics of opening a bond on the C_{60} surface, we optimized the C_{60} geometry using the MNDO method with selected bonds held open to fixed distances while the rest of the cage was allowed to relax. We have examined the opening of both types of bonds on C_{60}, between a pentagon and a hexagon (a 5–6 bond) and between two hexagons (6–6). A plot of the energy of each structure against the length of the open bond

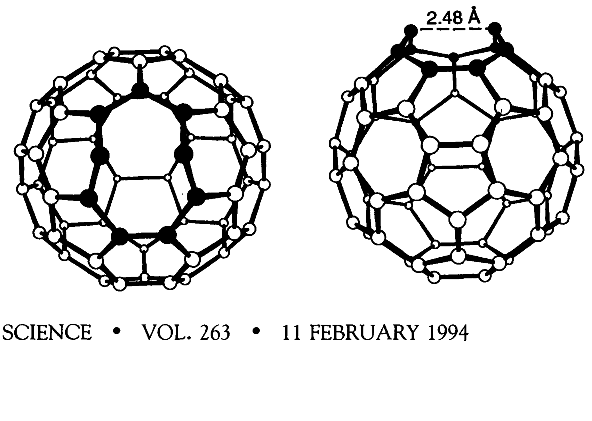

Fig. 1. The C_{60} window. By breaking a pentagon-hexagon bond on C_{60}, a large nine-membered ring is obtained. This structure with the bond open to 2.48 Å is a minimum on the MNDO unrestricted Hartree Fock (UHF) potential energy surface for the triplet state of C_{60}.

Department of Chemistry and Rice Quantum Institute, Rice University, Houston, TX 77251–1892, USA.

*To whom correspondence should be addressed.